Supplementary Information (SI) for Physical Chemistry Chemical Physics.

Electronic Supplementary information

Conductometric Evidence for Accurate Dissociation Behaviour of Surface Groups on Nanorods

Marcel Kröger[a]*, Kaarlo Nieminen[a], Han Tao[a] and Eero Kontturi[a]*

[a]Department of Bioproducts and Biosystems, Aalto University, FI-00076 Aalto, Finland

Table of Contents

Particle dimensions

Table S1. Dimensions of the particles as determined in our previous work.[1]

Dimension	Mean	Mode
Length	120.7 nm	116 nm
Height	10.7 nm	12.5 nm
Width	12.7 nm	

We adapted the values of the modes of the distributions in this work, as the number average dimensions of the particles are more representative in this study.

Reproducibility of titration experiments

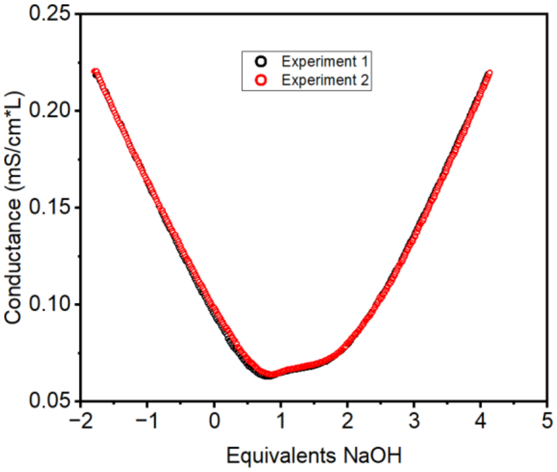

Figure S1. Reproducibility of the titration experiments. Larger discrepancies arise when the analyte volume changes significantly between experiments, as the dissociation equilibria depend on concentrations. Based on our experiments, this requires discrepancies larger than 5% (25mL), which can be actively avoided if necessary.

Titration of dispersed CNC vs modified pulp

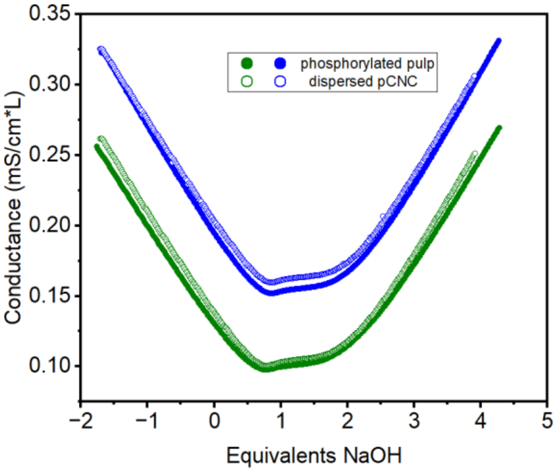

Figure S2. There are only slight discrepancies observable between dispersed CNC and modified pulp, suggesting that the diffusion of the particles has a negligible influence compared to the dissociation interactions, which in turn appear not to be dictated by the macroscopic order but the structure of the modified elemental fibrils. The green and blue curves are the same as in **Figure 9** (1.0 mM and 2.2 mM Cl^- background electrolyte).

Linearization analysis of conductometric titration curves of dissolved and immobilized phosphate

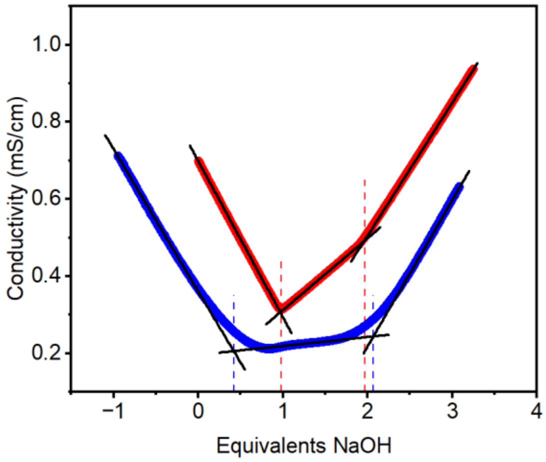

Figure S3. The analysis of the conductometric titration curve of phosphate surface groups on pCNC by linearization yields intersection points of individual segments that do not correspond to the equivalence points.

Dissociation constant of disodium hydrogen phosphate

The dissociation constant of disodium hydrogen phosphate was estimated by comparing the reaction to the dissociation of sodium dihydrogen phosphate (see, **Figure S4**). The foundation for this estimate is the following consideration.

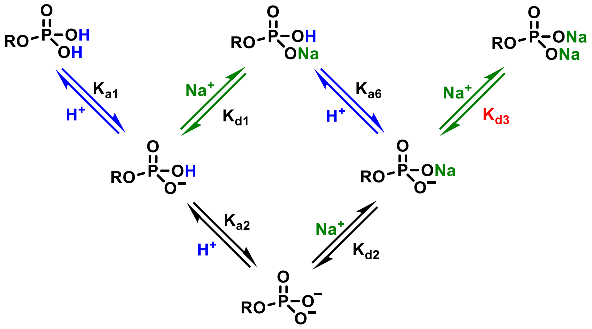

Figure S4. Dissociation reactions of interest of sodium hydrogen phosphates.

In both dissociation reactions characterized by K_{d1} and K_{d3}, one sodium ion is abstracted from the phosphate moiety. The difference is the charge of the phosphate moiety, given that the associated sodium ion is bound by an ionic bond, whereas the proton is bound by a covalent bond. Therefore, the electron density of the sodium phosphate moiety is notably higher compared to the hydrogen phosphate equivalent. This in turn influences the interaction of phosphate moiety and the ion dissociating ion in that it is easier to remove a sodium ion from mostly covalent hydrogen phosphate than partially ionic sodium phosphate. The same phenomenon is illustrated by the protolysis of fully protonated phosphoric acid and sodium dihydrogen phosphate. While the first pKa value of phosphoric acid is known to be 2.20, the perceived pKa value of sodium dihydrogen phosphate can be calculated as 5.32. The reduced acidity illustrates the stronger interactions of cation and partially ionic phosphate moiety.

Assuming that the free energy of the dissociation reactions of protons and sodium ions changes by the same relative amount, we can use the known decrease in acidity of the protolysis analogues to estimate the decrease in electrolytic strength for the dissociation reactions of sodium ions as described in equations **(S1)**, **(S2)** and **(S3)**.

$$\Delta G_{d3} = \Delta G_{d1} \cdot \frac{\Delta G_{a6}}{\Delta G_{a1}} \tag{S1}$$

$$-RT\ln K_{d3} = -RT\ln K_{d1} \cdot \frac{-RT\ln K_{a6}}{-RT\ln K_{a1}}$$

$$-\ln K_{d3} = -\ln K_{d1} \cdot \frac{-\ln K_{a6}}{-\ln K_{a1}}$$

$$-\frac{\ln K_{d3}}{\ln(10)} = -\frac{\ln K_{d1}}{\ln(10)} \cdot \frac{-\frac{\ln K_{a6}}{\ln(10)}}{-\frac{\ln K_{a1}}{\ln(10)}} \tag{S2}$$

$$pK_{d3} = pK_{d1} \cdot \frac{pK_{a6}}{pK_{a1}} = 0.65$$

$$K_{d3} = 0.22$$

$$\frac{1}{K_{d3}} = 4.5 \tag{S3}$$

This estimate is close to a previously published estimate for the sodium ion association to phosphate measured by the increase in acidity.[2] However, those experiments were carried out in the presence of tetramethylammonium ions as background electrolyte, which were assumed not to interact with the phosphate ions. The foundation for the obtained association constants is the pH change caused by ionic interactions of the phosphate ions, enhancing protolysis.[3]

Quantifying carbonate contaminants

The parameters required to solve **equation (25)** iteratively are the rate of the carbonation reaction and the carbonate content of the titrant. These can be determined in control experiments by the reduction in conductance caused by carbonate.

In order to assess the carbonation reaction, we measured the ageing of a sodium hydroxide solution over time by monitoring the conductivity decrease. This is shown in **Figure S5**.

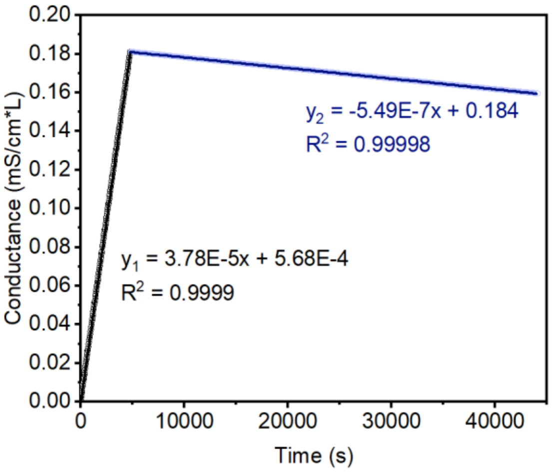

Figure S5. Conductivity decrease of basic analyte over time. 8mL 0.1M NaOH is dosed into 500mL degassed Milli-Q water at 1 ml/min as per the usual experimental setup, after which the analyte is left stirring overnight while monitoring the conductivity.

As the only cause of the decrease in conductance is the carbonation reaction and as the pH guarantees that it is in fact carbonate ions that are formed, it is possible to quantify the rate of carbonate formation by considering the slope of the curve as shown in equations **(S4)** and **(S5)**.

$$\frac{\Delta\sigma}{\Delta t} = r_{Carbonation}\left(\Lambda^0_{CO_3^{2-}} - 2\Lambda^0_{OH^-}\right) \tag{S4}$$

$$r_{Carbonation} = \frac{\frac{\Delta\sigma}{\Delta t}}{\left(\Lambda^0_{CO_3^{2-}} - 2\Lambda^0_{OH^-}\right)} = 2.50\frac{nmol}{s} \tag{S5}$$

Here, $\frac{\Delta\sigma}{\Delta t}$ is the conductivity decrease over time, $r_{Carbonation}$ is the time-dependent rate constant for the carbonation reaction.

This reaction rate is time dependent. For our purpose, it is more convenient, to express the passage of time by the rate of titrant addition. This way, it is possible to convert the rate of carbonation into a virtual concentration of carbonate being added to the analyte at the same rate as the titrant. This is expressed in equation **(S6)**.

$$[Carbonate]_{air} = \frac{r_{Carbonation}}{\frac{V_B}{t}} = \frac{r_{Carbonation}}{0.1\frac{mL}{min}} = r_{Carbonation} \cdot 600000\frac{s}{L} = 1.50\frac{mmol}{L} \tag{S6}$$

Here, $\frac{V_B}{t}$ is the dosing speed of the titrant during the titration.

If we assume that the carbonation reaction is occurring at this same speed during the dosing of the base into the degassed MilliQ water, it enables us to quantify the amount of carbonate contamination in the sodium hydroxide titrant solution according to equations **(S7)** and **(S8)**.

$$\begin{aligned}\Lambda_{base} &= \frac{\Delta\sigma}{\Delta c_B} = \frac{\Delta\sigma_{norm}}{\Delta n_B} = \Lambda_{Na^+} + (1-2\alpha)\Lambda_{OH^-} + \alpha\Lambda_{CO_3^{2-}} \\ &= \Lambda_{Na^+} + \left(1 - 2\frac{[Carbonate]_{NaOH} + [Carbonate]_{air}}{[base]}\right)\Lambda_{OH^-} \\ &\quad + \frac{[Carbonate]_{NaOH} + [Carbonate]_{air}}{[base]}\Lambda_{CO_3^{2-}}\end{aligned} \tag{S7}$$

$$[Carbonate]_{NaOH} = \frac{\Lambda_{base} - \Lambda^0_{Na^+} - \Lambda^0_{OH^-}}{\Lambda^0_{CO_3^{2-}} - 2\Lambda^0_{OH^-}}[base] - [Carbonate]_{air} = 2.50\frac{mmol}{L} \tag{S8}$$

Here, Λ_{base} is the molar limiting conductivity of the base, $\Delta\sigma$ is the difference in conductivity caused by changes in base concentration Δc_B, while, analogously, $\Delta\sigma_{norm}$ is the conductance decrease in response to changes in titrant amount Δn_B. α is the titer for carbonate in the system, which is the ratio of carbonate concentration versus assumed concentration of the base. $[Carbonate]_{NaOH}$ and $[Carbonate]_{air}$ are the concentrations of carbonate perceived in the titrant and in the air, entering the analyte in the timeframe of the addition of one increment of base, and $[base]$ is the concentration of the titrant.

Both sources of carbonate can be expressed as contained in the titrant and therefore quantified along with the titrant along the course of the titration.

Details on the composition of the simulated experiments

Table S2. Compositions of the simulated titration experiments.

		HCl	**NaCl**	**pCNC**	**initial mass**	**background ionic strength (mmol)**	**Titer of NaOH solution**
0.4 mM Cl$^-$	**g**	1.97	0	0.2882	509.61	0.197	1
	mmol	0.197	0	0.2882			
	eq	0.7	0	1			
1.0 mM Cl$^-$	**g**	4.97	0	0.2700	495.41	0.497	1
	mmol	0.497	0	0.2700			
	eq	1.8	0	1			
1.6 mM Cl$^-$	**g**	5.63	0.5	0.2838	505.77	0.813	1
	mmol	0.563	0.25	0.2838			
	eq	2.0	0.9	1			
2.2 mM Cl$^-$	**g**	4.97	1.52	0.2998	568.10	1.257	1
	mmol	0.497	0.76	0.2998			
	eq	1.7	2.5	1			

Triple amount CNC, 1.6 mM Cl^-	**g**	8.18	0	0.8656	519.00	0.818	0.95$^{a)}$
	mmol	0.818	0	0.8656			
	eq	0.9	0	1			
Ionic phosphate, 1.6 mM Cl^-	**g**	8.56	0	0.8560	525.90	0.856 + nearly quantitiatively dissociated sodium dihydrogen phosphate	0.95$^{a)}$
	mmol	0.856	0	0.8560			
	eq	1	0	1			

a) When absent-mindedly diluting 1M NaOH solution by weight instead of by volume, the slightly elevated density of 1M NaOH causes a discrepancy in the final concentration of 5%.

Appendix A: Estimation of the counterion condensation equilibrium constant

As discussed above and shown in **Figure 1**, we assume that the electrostatic surface energy, which inhibits the dissociation of the surface groups, is an additive component of the overall reaction free energy. Consequently, the dissociation equilibria are shifted towards association, which can be expressed in an updated equilibrium constant according to **equation (A1).**[4]

$$K_{new} = e^{-\frac{\Delta G^0_{dissociation} + U}{k_B T}} = e^{-\frac{\Delta G^0_{dissociation}}{k_B T}} \cdot e^{-\frac{U}{k_B T}} = K_{dissociation} \cdot K_{condensation} \qquad \textbf{(A1)}$$

We are assuming here, that the free energy resulting from the dissociation reaction of the surface groups, $\Delta G^0_{dissociation}$, remains constant, but that it is the external effect of the surrounding electrostatic surface energy, that accounts for the shift in the reaction equilibrium. This is not entirely factual. In the colloidal system, the entropy gain will be reduced on account of ions being trapped in the electrostatic double layer. As for the reaction enthalpy, on the back of NMR studies showing no significant shift of the phosphate signal of phosphate half-esters and orthophosphate,[1, 5] we can assume that the shielding of the central phosphorous atom of surface groups and that of phosphate ions are nearly equal, which then translates to the dissociation constants being nearly equal. Also, there is precedent for the separate contemplation of the ionic interactions between the two dissociating charges and the electrostatic background.[6, 7]

Still, this methodology is at odds with Manning's previous work[8]. There, reaction enthalpy and electrostatic surface contributions are contracted to give an electric free energy, which is distinct from a second energetic influence: translational entropy of the dissociated ions. Manning's ab initio methodology, however, still relies on mathematical simplifications in order to be readily computed and only takes into account a single ion species dissociating from the polyelectrolyte. Given our application, we need to account for at least two ion species in interconnected dissociation equilibria. Therefore, our semi-empirical approach sacrifices a small degree of thermodynamical accuracy for far easier computation and significantly increased adaptability.

In order to quantify the correction factor to the equilibrium constants in **equation (2)**, it is necessary to describe the electrostatic potential of the surrounding charges. In the presence of background electrolyte, according to Debye and Hückel, the potential of a point described with **equation (A2)**.[7] The key parameter here is the screening parameter, the inverse of the Debye length, which is calculated according to **equation (A3)**.

$$\varphi = \frac{N_q q_e}{4\pi\varepsilon_0\varepsilon_r}\frac{e^{\kappa r_{ion}}}{(1+\kappa r_{ion})}\frac{e^{-\kappa d}}{d} \tag{A2}$$

$$\kappa = \frac{1}{\lambda_D} = \sqrt{\frac{2{q_e}^2 I}{\varepsilon_0\varepsilon_r k_B T}} \tag{A3}$$

Here, φ is the electrostatic potential, N_q is the number of elemental charges of an ion with radius r_{ion}, that a probing charge at a distance d interacts with, and κ is the Debye screening parameter.

The screening parameter is the inverse of the Debye Length λ_D, which depends on the ionic strenght I of the solution.

Such a potential affects the electrostatic potential energy U between a symbolic, probing point charge and the charge generating the potential according to equation **(A4)**:

$$U = \frac{1}{2} q_{probe}\frac{N_q q_e}{4\pi\varepsilon_0\varepsilon_r}\frac{e^{\kappa r_{ion}}}{(1+\kappa r_{ion})}\frac{e^{-\kappa d}}{d} \tag{A4}$$

The overall electrostatic potential energy of a single charge originating from multiple nearby charges is obtained by summing up all individual contributions.

For our purpose, we need to determine the electrostatic energy U in **equation (2)**, which describes the additional electrostatic energy that inhibits the dissociation process. This energy is caused by all nearby surface charges except for the one charge that is part of the dissociating ion pair. As such, we need to consider the sum of the screened potential contributions of all surface charges on the particle, which are causing an electrostatic potential on the screened charge of a single ion in a surface ion pair. The electrostatic interactions of this ion pair can be neglected, since, in **equation (2)**, these interactions are described through the regular ion dissociation constant, which we are merely trying to modify. As such, the additional electrostatic energy can be calculated according to **equation (A5)**:

$$
\begin{aligned}
U &= \frac{1}{2}\sum_i q_{probe}\frac{N_{q,i}q_e}{4\pi\varepsilon_0\varepsilon_r}\frac{e^{\kappa r_{ion}}}{(1+\kappa r_{ion})}\frac{e^{-\kappa d_i}}{d_i} \\
&= \frac{1}{2}\frac{1}{4\pi\varepsilon_0\varepsilon_r}\frac{e^{\kappa r_{ion}}}{(1+\kappa r_{ion})}\sum_i \frac{q_{probe}N_{q,i}q_e e^{-\kappa d_i}}{d_i} \\
&= \frac{1}{2}\frac{{q_e}^2}{4\pi\varepsilon_0\varepsilon_r}\frac{e^{\kappa r_{ion}}}{(1+\kappa r_{ion})}\sum_i \frac{N_{q,i}e^{-\kappa d_i}}{d_i}
\end{aligned}
\tag{A5}
$$

This description of the electric potential energy depends on the distance of the considered charges. This is not trivial, as the number of charges is varying along the titration process and the distances between the charges is hard to assess given the rather complicated arrangement of the functional groups along cellulose nanocrystals. Therefore, we consider several simplifications: We will consider the CNC to have cylindrical shape and symmetry, as well as a uniform surface charge σ located on the mantle area, which can be calculated via **equation (A6)**:

$$
\begin{aligned}
\sigma_S &= \frac{N_q}{A_P} = \frac{N_q}{2\pi r_p l} \\
&= \frac{N_A\sigma_m}{2\pi r_p l}m_p \\
&= \frac{N_A\sigma_m}{2\pi r_p l}\rho V_p \\
&= \frac{N_A\sigma_m}{2\pi r_p l}\rho\pi r_p^2 l \\
&= \frac{N_A q_e \sigma_m \rho r_p}{2}
\end{aligned}
\tag{A6}
$$

Here, Q is the total charge of the particle, A_P is the surface area of the particle that we simplify to the mantle area of the cylindrical particle, r_p is the particle radius, l is the particle length, σ_m is specific charge density of the cellulose particles and ρ is the density of cellulose.

With this assumption of a uniform charge density in mind, the potential of a single point on the surface of the cylindrical particle against the rest of the particle surface relies on the area of the considered segments, which determines the contained charge, and their Euclidian distance, which determines the magnitude of the interaction.

In order to calculate this, we describe the cylindrical particle with respect to a single point on its surface, which is located in the origin of a cartesian coordinate system. As such, the z-axis describes the length of the cylinder and lies on its surface, while the x-axis aligns with the diameter of the cylinder as shown in **Figure A1**.

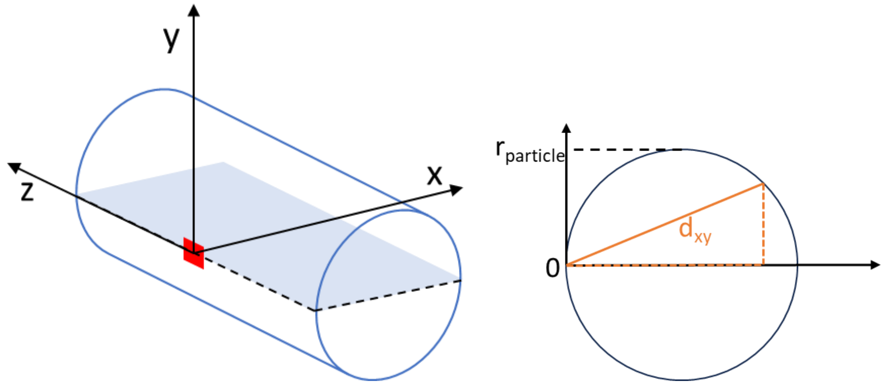

Figure A1. Orientation of the cylindrical particle in the coordinate system chosen to describe the electrostatic interactions of an elementary charge located at the origin (left). The electrostatic interactions are evaluated based on the distance d of surface area elements to the considered charge located at the origin (right).

The Euclidian distance of any point from the origin of this coordinate system can be described by 3-dimensional Pythagorean deliberations as follows:

Considering the x-y-plane, **equation (A7)** expresses the y-coordinate of the cylinder surface as a function of the particle radius and x-coordinate, while **equation (A8)** describes the two-dimensional Euclidean distance d_{xy} of every point from the z-axis:

$$r_p{}^2 = \left(x - r_p\right)^2 + y^2$$

$$y = \sqrt{r_p{}^2 - \left(x - r_p\right)^2} = \sqrt{r_p{}^2 - \left(r_p{}^2 - 2xr_p + x^2\right)} = \sqrt{2xr_p - x^2} \quad \textbf{(A7)}$$

$$d_{xy} = \sqrt{x^2 + y^2} = \sqrt{x^2 + 2xr_p - x^2} = \sqrt{2xr_p} \quad \textbf{(A8)}$$

Equation (A8) can be extended to describe the 3-dimensional Euclidean distance d_{3D} of any surface point from the origin of our coordinate system according to **equation (A9)**.

$$d_{3D} = \sqrt{d_{xy}{}^2 + z^2} = \sqrt{2xr_p + z^2} \quad \textbf{(A9)}$$

In order to assess the electrostatic potential contribution of a point on the cylinder surface at a distance d_{3D}, we now need to consider the charge in the respective point. The charge is given by the product of the surface charge density σ and area increment of the point i as follows in **equation (A10)**.

$$N_{q,i} q_e = \sigma_S \cdot dA_i \quad \textbf{(A10)}$$

$$dA = dzd_{arc} = dz\sqrt{dx^2 + dy^2} = dz\sqrt{dx^2 + \left(\frac{d}{dx}\left(\sqrt{2xr_p - x^2}\right)dx\right)^2}$$

with

$$\begin{aligned} &= dzdx\sqrt{1 + \left(\frac{x - r_p}{\sqrt{2xr_p - x^2}}\right)^2} = dzdx\sqrt{1 + \frac{\left(x - r_p\right)^2}{2xr_p - x^2}} \\ &= dzdx\sqrt{\frac{2xr_p - x^2 + \left(x - r_p\right)^2}{2xr_p - x^2}} \\ &= dzdx\sqrt{\frac{r_p{}^2 + 2xr_p - 2xr_p + x^2 - x^2}{2xr_p - x^2}} = \frac{r_p}{\sqrt{2xr_p - x^2}}dzdx \end{aligned} \tag{A11}$$

By considering the infinitesimal area increments described in **equation (A11)**, the sum in equation ((A5) can be transformed into an integral. The boundaries for the integration in x-direction are the boundaries of the considered charge and the particle, respectively, with $x_{min} = x_{ch}$ and $x_{max} = 2r_p$. In z-direction two separate integrations can be performed, both originating at $z_{min} = z_{ch}$ and proceeding to either end of the particle at $z_{max,1} = z''$ and $z_{max,2} = (l - z')$.

The boundary of the considered charge can be derived from the charge density. For the sake of simplicity, given the choice of a cartesian coordinate system, we assume the shape of the charge to be a square in the yz-plane, with the center of the square located at the origin of the coordinate system and spanning the area A_{ch}. This means that both x_{ch} and z_{ch} can be calculated according to the following **equations (A12)**, **(A13)** and **(A14)**.

$$A_{ch} = \frac{1}{\sigma_S} = \frac{2}{q_e \sigma_m \rho r_p} = (2z_{ch})^2 = (2y_{ch})^2 \tag{A12}$$

$$z_{ch} = \sqrt{\frac{1}{2q_e\sigma_m\rho r_p}} \tag{A13}$$

(From above:)

$$y = \sqrt{2xr_p - x^2} \Leftrightarrow x = r_p - \sqrt{{r_p}^2 - y^2} \tag{A7}$$

$$x_{ch} = r_p - \sqrt{{r_p}^2 - \frac{1}{2q_e\sigma_m\rho r_p}} \tag{A14}$$

For the sake of simplicity, however, we will assume that the boundary of the charge is found at $z_{ch} = 3\ \text{Å}$ from the center, which corresponds to the hydration radius of a phosphate ion. This saves time during the calculation by omitting one recursive calculation at the core of our model while still being reasonably accurate.

Two more aspects need to be considered. Firstly, given the non-negative output of square root operations, only the top half of the cylinder is considered by **equation (A7)**. The described integrations return a surface area for the top half of the cylinder that satisfies y>0. The second half of the cylinder is considered through symmetry by adding a factor of 2.

Secondly and lastly, the electrical energy between the charge in the origin of our calculations and the charged surface scales with the magnitude of the surrounding charges and their distance, as discussed above and described in **equation (3)**. We have described how to assess the distance of any point on the particle surface in **equation (A9)** and how to assess the charge of a given surface area increment on the basis of the surface charge density in **equations (A10)** and **(A11)**. However, by describing the area increments in **equation (A11)** as a function of increments in x and z, we consider area increments of varying size and therefore varying charge at a given distance d_{3D} from the origin. This is illustrated in **Figure A2**.

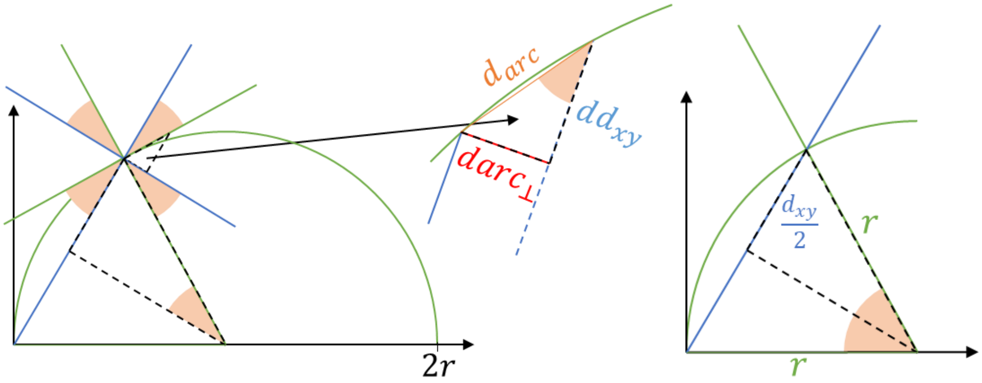

Figure A2. Discrepancy between assumed and actual location of the considered surface charge in an area increment at $x \ll r$ and parameters used to define the orthogonal component $d_{arc_{\perp}}$.

Especially at $x \ll r$, the calculated change in arc length d_{arc} for an increment in x-direction is similar to the change in distance from the origin dd_{xy}. This means that the comparison between charge amount on the surface and distance from the origin as required by **equation (3)** is not accurately reflected in our deliberations. Instead, given the choice of cartesian coordinates, we overestimate the charge close to the origin in **equation (A11)** by considering larger surface area increments. In order to rectify this misconception, we consider the orthogonal component of the arc length instead, which translates to an orthogonal component of the charge, that is accurately scaled in its distance from the origin. This requires an amendment according to **equation (A15)**.

$$d_{arc_{\perp}} = d_{arc}\frac{d_{xy}}{2r_p}$$

$$= d_{arc}\frac{\sqrt{2xr_p}}{2r_p} \qquad \textbf{(A15)}$$

$$= \frac{r_p}{\sqrt{2xr_p - x^2}} dx \frac{\sqrt{2xr_p}}{2r_p}$$

$$= \sqrt{\frac{x}{2r_p}} \frac{r_p}{\sqrt{2xr_p - x^2}} dx$$

$$= \sqrt{\frac{r_p}{4r_p - 2x}} dx$$

As such, combining **equations (A5)** to **(A15)** yields equation **(A16)**, which describes the electrostatic potential energy for a charge located at a distance z = z’ from either end of the particle.

$$\begin{aligned} U_{z'} &= \frac{1}{2} \frac{{q_e}^2}{4\pi\varepsilon_0\varepsilon_r} \frac{e^{\kappa r_{ion}}}{(1+\kappa r_{ion})} \left(\int_0^{z'} \int_0^{2r_p} 2\sqrt{\frac{r_p}{4r_p - 2x}} \frac{\sigma_S}{\sqrt{2xr_p + z^2}} e^{-\kappa\sqrt{2xr_p+z^2}} dxdz \right. \\ &+ \int_0^{l-z'} \int_0^{2r_p} 2\sqrt{\frac{r_p}{4r_p - 2x}} \frac{\sigma_S}{\sqrt{2xr_p + z^2}} e^{-\kappa\sqrt{2xr_p+z^2}} dxdz \\ &\left. - 2\int_0^{z_{ch}} \int_0^{x_{ch}} 2\sqrt{\frac{r_p}{4r_p - 2x}} \frac{\sigma}{\sqrt{2xr_p + z^2}} e^{-\kappa\sqrt{2xr_p+z^2}} dxdz \right) \end{aligned} \quad \textbf{(A16)}$$

$$\begin{aligned} &= \frac{{q_e}^2\sigma_S}{4\pi\varepsilon_0\varepsilon_r} \frac{e^{\kappa r_{ion}}}{(1+\kappa r_{ion})} \left(\int_0^{z'} \int_0^{2r_p} \sqrt{\frac{2r_p}{2r_p - x}} \frac{1}{\sqrt{2xr_p + z^2}} e^{-\kappa\sqrt{2xr_p+z^2}} dxdz \right. \\ &\qquad + \int_0^{l-z'} \int_0^{2r_p} \sqrt{\frac{2r_p}{2r_p - x}} \frac{1}{\sqrt{2xr_p + z^2}} e^{-\kappa\sqrt{2xr_p+z^2}} dxdz \\ &\qquad \left. - 2\int_0^{z_{ch}} \int_0^{x_{ch}} \sqrt{\frac{2r_p}{2r_p - x}} \frac{1}{\sqrt{2xr_p + z^2}} e^{-\kappa\sqrt{2xr_p+z^2}} dxdz \right) \end{aligned}$$

$$= \frac{{q_e}^2 \sigma_S}{4\pi\varepsilon_0\varepsilon_r} \frac{e^{\kappa r_{ion}}}{(1+\kappa r_{ion})} \left(\int_0^{z\prime} \int_0^{2r_p} \sqrt{\frac{2r_p}{(2r_p - x)(2xr_p + z^2)}} e^{-\kappa\sqrt{2xr_p+z^2}} dxdz \right.$$

$$+ \int_0^{l-z\prime} \int_0^{2r_p} \sqrt{\frac{2r_p}{(2r_p - x)(2xr_p + z^2)}} e^{-\kappa\sqrt{2xr_p+z^2}} dxdz$$

$$\left. - 2\int_0^{z_{ch}} \int_0^{x_{ch}} \sqrt{\frac{2r_p}{(2r_p - x)(2xr_p + z^2)}} e^{-\kappa\sqrt{2xr_p+z^2}} dxdz \right)$$

At this point, in order to abbreviate the integral term, we define **equation (A17)**.

$$\Psi(z') = \int_0^{z'} \int_0^{2r_p} \sqrt{\frac{2r_p}{(2r_p - x)(2xr_p + z^2)}} e^{-\kappa\sqrt{2xr_p+z^2}} dxdz$$

$$+ \int_0^{l-z'} \int_0^{2r_p} \sqrt{\frac{2r_p}{(2r_p - x)(2xr_p + z^2)}} e^{-\kappa\sqrt{2xr_p+z^2}} dxdz \qquad \textbf{(A17)}$$

$$- 2\int_0^{z_{ch}} \int_0^{x_{ch}} \sqrt{\frac{2r_p}{(2r_p - x)(2xr_p + z^2)}} e^{-\kappa\sqrt{2xr_p+z^2}} dxdz$$

Expressing equation (A16 in thermal units yields equation (A18:

$$\frac{U_{z'}}{k_BT} = \frac{{q_e}^2}{4\pi\varepsilon_0\varepsilon_r k_BT} \sigma_S \cdot \Psi(z') \qquad \textbf{(A18)}$$

$$= \lambda_B \sigma \cdot \Psi(z')$$

The integral term abbreviated as $\Psi(z')$ contains the information about the magnitude of the screened charges and their distance and can therefore be considered as a geometric normalization factor. Meanwhile, the product of Bjerrum length and charge density echoes Manning’s deliberations.

The electrostatic potential energy $U_{z\prime}$ of a single charge varies as a function of that charges position on the nanocrystal z’. Charges located at either end of the particle are surrounded by fewer neighboring charges than those located in the middle of the particle. This variation in distance causes a discrepancy in the electrostatic potential energy, resulting in a maximum for those charges located exactly in the middle of the particle, as shown in **Figure A3.** As far as we can tell, this effect is considered in works on charge renormalization through the geometric shape and symmetry of the colloidal particles when applying the Poisson-Boltzmann equation.[9, 10] In that formalism, splitting the contributions of a single groups against the remaining surface is not necessary. Nevertheless, it might be the combination of both ion condensation and the screening effects of ions in the double layer, rather than just the former effect alone, that makes charge renormalization necessary in the first place.

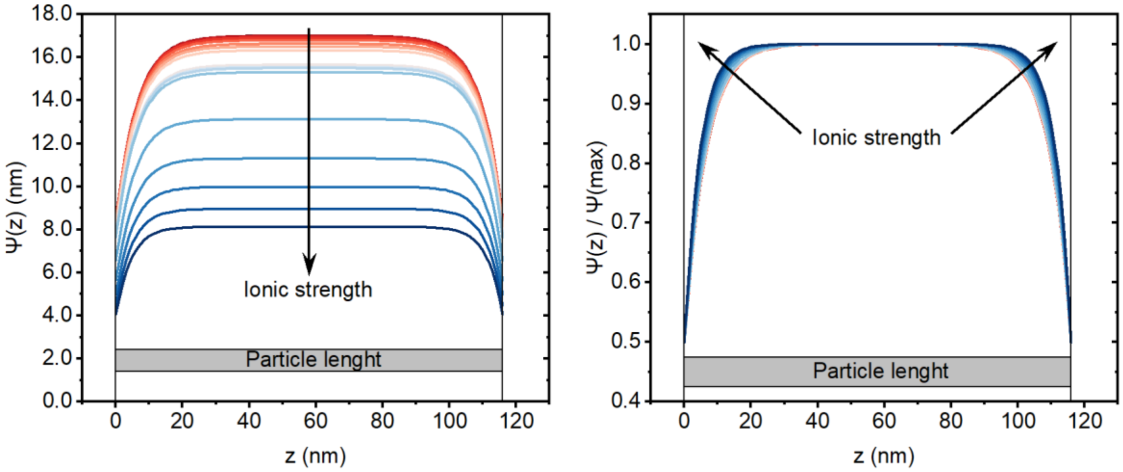

Figure A3. Absolute (left) and relative (right) values for $\Psi(z')\, over\, z'$, for 17 evenly spaced points along the titration curve. Both absolute and relative values vary in response to the ionic strength, which rises quickly after the second equivalence point and promotes screening of the surface charge.

The shape of the curves in **Figure A3** illustrates that, while the absolute values of the charge change, the relative overall potential remains the same. Also, the potential drops off only in the last 20nm of the particle at either end, which illustrates that the contributions of charges located more than 25nm from the considered origin have no further effect on the local surface potential. As such, the center section of the particles can be considered as having a uniform, cylindrical surface potential. For our model, to avoid having to calculate this integral for every value of z’, we will consider the average value for the electrostatic potential energy across all z’, which amounts to 94.5% of the maximum value for $z' = \frac{l}{2}$.

This means that our counterion condensation correction to the conventional equilibrium constant can be expressed according to **equation (A19).**

$$K_{condensation} = e^{-\frac{U}{k_B T}} = e^{-\frac{\lambda_B}{\left(\frac{1\ A}{r_p N_i}\right)} \cdot \Psi(z')} \tag{A19}$$

Finally, by combining **equations (2)** and **(A19)**, we can describe the effective dissociation constants of the surface groups quantitatively.

Appendix B: Matrix expression of the equilibrium concentrations

The individual concentrations of the 15 relevant species in our system are fully defined by the set of 15 equations (see, **equations (10)** to **(24)**) defined above. This becomes more evident and far easier to handle by expressing the set of individual equations in a single matrix equation.

Obviously, while the mass and charge balances in equations **(10)** to **(13)** and **(23)**, respectively, are linear, whereas the remaining **equations (14)** to **(22)** and **(24)**, which contain the information on the dissociation equilibria are not linear. This illustrates that the system cannot be solved by Gaussian elimination, but, instead, requires numerical approaches. Therefore, it is useful to consider logarithmic concentrations instead of absolute values, which ensures that the solution provides no negative values as concentrations. The more significant benefit of the logarithmic form is that 10 out of 15 expressions, containing the information about the equilibrium constants, become linear, as shown in **equation (B1)**.

$$\begin{pmatrix} 1 & 0 & 0 & 1 & 0 & 0 & 0 & 0 & 0 & 0 & 0 & 0 & 0 & 0 & 0 \\ 1 & 0 & 0 & 0 & -1 & 1 & 0 & 0 & 0 & 0 & 0 & 0 & 0 & 0 & 0 \\ 1 & 0 & 0 & 0 & 0 & -1 & 1 & 0 & 0 & 0 & 0 & 0 & 0 & 0 & 0 \\ 0 & 1 & 0 & 0 & 0 & 1 & 0 & -1 & 0 & 0 & 0 & 0 & 0 & 0 & 0 \\ 0 & 1 & 0 & 0 & 0 & 0 & 1 & 0 & -1 & 0 & 0 & 0 & 0 & 0 & 0 \\ 0 & 1 & 0 & 0 & 0 & 0 & 0 & 0 & 1 & -1 & 0 & 0 & 0 & 0 & 0 \\ 1 & 0 & 0 & 0 & 0 & 0 & 0 & 0 & 0 & 0 & -1 & 1 & 0 & 0 & 0 \\ 1 & 0 & 0 & 0 & 0 & 0 & 0 & 0 & 0 & 0 & 0 & -1 & 1 & 0 & 0 \\ 0 & 1 & 0 & 0 & 0 & 0 & 0 & 0 & 0 & 0 & 0 & 1 & 0 & -1 & 0 \\ 0 & 1 & 0 & 0 & 0 & 0 & 0 & 0 & 0 & 0 & 0 & 0 & 1 & 0 & -1 \end{pmatrix} \times \begin{pmatrix} ln[H^+] \\ ln[Na^+] \\ ln[Cl^-] \\ ln[OH^-] \\ ln[H_2RPO_4] \\ ln[HRPO_4^-] \\ ln[RPO_4^{2-}] \\ ln[HNaRPO_4] \\ ln[NaRPO_4^-] \\ ln[Na_2RPO_4] \\ ln[CO_{2,aq}] \\ ln[HCO_3^-] \\ ln[CO_3^{2-}] \\ ln[NaHCO_3] \\ ln[NaCO_3^-] \end{pmatrix} = \begin{pmatrix} ln\, K_w \\ ln\, K_{a1} + ln\, K_{cc} \\ ln\, K_{a2} + ln\, K_{cc} \\ ln\, K_{d1} + ln\, K_{cc} \\ ln\, K_{d2} + ln\, K_{cc} \\ ln\, K_{d3} + ln\, K_{cc} \\ ln\, K_{a4} \\ ln\, K_{a5} \\ ln\, K_{d4} \\ ln\, K_{d5} \end{pmatrix} \qquad \textbf{(B1)}$$

For the remaining 5 mass and charge balances, a redundant dependence on the logarithmic concentrations can be introduced by expressing the real concentrations as exponentials of their own logarithms and by multiplying with the expression $\frac{\ln[i]}{\ln[i]} = 1$. The resulting expanded expressions are shown in **equations (B2)**, **(B3)**, **(B4)**, **(B5)** and **(B6)**.

$$[\Sigma(Chloride)] = \frac{e^{ln[Cl^-]}}{ln[Cl^-]} \cdot ln[Cl^-] \qquad \textbf{(B2)}$$

$$\begin{aligned} [\Sigma(Sodium)] = {} & \frac{e^{ln[Na^+]}}{ln[Na^+]} \cdot ln[Na^+] + \frac{e^{ln[HNaRPO_4]}}{ln[HNaRPO_4]} \cdot ln[HNaRPO_4] + \frac{e^{ln[NaRPO_4^-]}}{ln[NaRPO_4^-]} \cdot ln[NaRPO_4^-] \\ & +2\frac{e^{ln[Na_2RPO_4]}}{ln[Na_2RPO_4]} \cdot ln[Na_2RPO_4] + \frac{e^{ln[NaHCO_3]}}{ln[NaHCO_3]} \cdot ln[NaHCO_3] + \frac{e^{ln[NaCO_3^-]}}{ln[NaCO_3^-]} \cdot ln[NaCO_3^-] \end{aligned} \qquad \textbf{(B3)}$$

$$\begin{aligned} [\Sigma(Phosphate)] = {} & \frac{e^{ln[H_2RPO_4]}}{ln[H_2RPO_4]} \cdot ln[H_2RPO_4] + \frac{e^{ln[HRPO_4^-]}}{ln[HRPO_4^-]} \cdot ln[HRPO_4^-] + \frac{e^{ln[RPO_4^{2-}]}}{ln[RPO_4^{2-}]} \cdot ln[RPO_4^{2-}] \\ & + \frac{e^{ln[HNaRPO_4]}}{ln[HNaRPO_4]} \cdot ln[HNaRPO_4] + \frac{e^{ln[NaRPO_4^-]}}{ln[NaRPO_4^-]} \cdot ln[NaRPO_4^-] + \frac{e^{ln[Na_2RPO_4]}}{ln[Na_2RPO_4]} \cdot ln[Na_2RPO_4] \end{aligned} \qquad \textbf{(B4)}$$

$$[\Sigma(Carbonate)] = \frac{e^{ln[CO_{2,aq}]}}{ln[CO_{2,aq}]} \cdot ln[CO_{2,aq}] + \frac{e^{ln[HCO_3^-]}}{ln[HCO_3^-]} \cdot ln[HCO_3^-] + \frac{e^{ln[CO_3^{2-}]}}{ln[CO_3^{2-}]} \cdot ln[CO_3^{2-}] + \frac{e^{ln[NaHCO_3]}}{ln[NaHCO_3]} \cdot ln[NaHCO_3] + \frac{e^{ln[NaCO_3^-]}}{ln[NaCO_3^-]} \cdot ln[NaCO_3^-] \tag{B5}$$

$$0 = \left(\frac{e^{ln[H^+]}}{ln[H^+]} \cdot ln[H^+] + \frac{e^{ln[Na^+]}}{ln[Na^+]} \cdot ln[Na^+]\right) - \left(\frac{e^{ln[Cl^-]}}{ln[Cl^-]} \cdot ln[Cl^-] + \frac{e^{ln[OH^-]}}{ln[OH^-]} \cdot ln[OH^-] + \frac{e^{ln[HRPO_4^-]}}{ln[HRPO_4^-]} \cdot ln[HRPO_4^-] + 2\frac{e^{ln[RPO_4^{2-}]}}{ln[RPO_4^{2-}]} \cdot ln[RPO_4^{2-}] + \frac{e^{ln[NaRPO_4^-]}}{ln[NaRPO_4^-]} \cdot ln[NaRPO_4^-] + \frac{e^{ln[HCO_3^-]}}{ln[HCO_3^-]} \cdot ln[HCO_3^-] + \frac{e^{ln[NaCO_3^-]}}{ln[NaCO_3^-]} \cdot ln[NaCO_3^-] + 2\frac{e^{ln[CO_3^{2-}]}}{ln[CO_3^{2-}]} \cdot ln[CO_3^{2-}]\right) \tag{B6}$$

To apply these equations to our titrations, it must be considered, that the overall concentrations in **equations (B2)** to **(B5)** vary due to dilution and in the case of **(B3)** due to the active increase in total sodium concentration when sodium hydroxide is added to the system. These dependencies can be expressed according to **equations (B7)**, **(B8)**, **(B9)** and **(B10)**.

$$[\Sigma(Chloride)] = [Chloride]_0\left(\frac{V_0}{V_0+V_B}\right) = c_{HCl}\left(\frac{V_{HCl}}{V_0+V_B}\right) + c_{NaCl}\left(\frac{V_{NaCl}}{V_0+V_B}\right) \tag{B7}$$

$$[\Sigma(Sodium)] = [Sodium]_0\left(\frac{V_0}{V_0+V_B}\right) + c_B\left(\frac{V_B}{V_0+V_B}\right) = c_{NaCl}\left(\frac{V_{NaCl}}{V_0+V_B}\right) + \upsilon\varrho_P\left(\frac{m_{CNC}}{V_0+V_B}\right) + c_B\left(\frac{V_B}{V_0+V_B}\right) \tag{B8}$$

$$[\Sigma(Phosphate)] = [Phosphate]_0\left(\frac{V_0}{V_0+V_B}\right) = \varrho_P\left(\frac{m_{CNC}}{V_0+V_B}\right) \tag{B9}$$

$$[\Sigma(Carbonate)] = [Carbonate]_{v_B}\left(\frac{V_0}{V_0+V_B}\right) = \left(c_{CO_3^{2-}}^{air} + c_{CO_3^{2-}}^{base}\right)\left(\frac{V_B}{V_0+V_B}\right) \tag{B10}$$

In **equations (B7)**, **(B8)**, **(B9)** and **(B10)**, V_0 is the starting volume of the analyte solution and V_B is the volume of added base throughout the titration. c_{HCl}, c_{NaCl} and c_B are the concentrations of HCl, NaCl and sodium hydroxide solutions, which are added to the analyte during sample preparation and titration, respectively. The volumina of HCl and NaCl solutions added to the analyte contribute to the starting volume V_0. $c_{CO_3^{2-}}^{air}$ and $c_{CO_3^{2-}}^{base}$ describe the amount of carbonate contamination present in the sodium hydroxide solution and entering the analyte from the air and are expressed as concentrations of the sodium hydroxide solution as explained in the supplement. ϱ_P is the specific phosphate content (mol/kg) of the cellulose analyte, υ is the degree of neutralization of the phosphate groups (0 for full protonation, 2 for full deprotonation) and m_{CNC} is the mass (kg) of cellulose phosphate in the analyte solution.

Additionally, the value of the counterion condensation constant K_{cc} (as defined in **equation (A19)**) changes in response to the ionic strength and active surface charge. Therefore, while it is a constant at individual equilibrium conditions, it assumes different values for every datapoint along the titration curves in response to the changes in surface protonation and ionic strength.

With these information, we can define the matrix **M** according to **equation (B11)** and a volume dependent vector **K(**$\boldsymbol{V_B}$**)** according to **equation (B12)**, which enable us to numerically find a solution for the logarithmic concentration vector $\boldsymbol{C_{ln}}$ (see, **equation (B13)**) according to **equation (25)**.

$$\boldsymbol{C_{ln}}(\boldsymbol{V_B}) = \boldsymbol{M}^{-1} \times \boldsymbol{K}(\boldsymbol{V_B}) \tag{25}$$

$$
\boldsymbol{M} = \begin{pmatrix}
1 & 0 & 0 & 1 & 0 & 0 & 0 & 0 & 0 & 0 & 0 & 0 & 0 & 0 & 0 \\
1 & 0 & 0 & 0 & -1 & 1 & 0 & 0 & 0 & 0 & 0 & 0 & 0 & 0 & 0 \\
1 & 0 & 0 & 0 & 0 & -1 & 1 & 0 & 0 & 0 & 0 & 0 & 0 & 0 & 0 \\
0 & 1 & 0 & 0 & 0 & 1 & 0 & -1 & 0 & 0 & 0 & 0 & 0 & 0 & 0 \\
0 & 1 & 0 & 0 & 0 & 0 & 1 & 0 & -1 & 0 & 0 & 0 & 0 & 0 & 0 \\
0 & 1 & 0 & 0 & 0 & 0 & 0 & 0 & 1 & -1 & 0 & 0 & 0 & 0 & 0 \\
1 & 0 & 0 & 0 & 0 & 0 & 0 & 0 & 0 & 0 & -1 & 1 & 0 & 0 & 0 \\
1 & 0 & 0 & 0 & 0 & 0 & 0 & 0 & 0 & 0 & 0 & -1 & 1 & 0 & 0 \\
0 & 1 & 0 & 0 & 0 & 0 & 0 & 0 & 0 & 0 & 0 & 1 & 0 & -1 & 0 \\
0 & 1 & 0 & 0 & 0 & 0 & 0 & 0 & 0 & 0 & 0 & 0 & 1 & 0 & -1 \\
0 & \frac{e^{ln[Na^+]}}{ln[Na^+]} & 0 & 0 & 0 & 0 & 0 & \frac{e^{ln[HNaRPO_4]}}{ln[HNaRPO_4]} & \frac{e^{ln[NaRPO_4^-]}}{ln[NaRPO_4^-]} & 2\frac{e^{ln[Na_2RPO_4]}}{ln[Na_2RPO_4]} & 0 & 0 & 0 & \frac{e^{ln[NaHCO_3]}}{ln[NaHCO_3]} & \frac{e^{ln[NaCO_3^-]}}{ln[NaCO_3^-]} \\
0 & 0 & \frac{e^{ln[Cl^-]}}{ln[Cl^-]} & 0 & 0 & 0 & 0 & 0 & 0 & 0 & 0 & 0 & 0 & 0 & 0 \\
0 & 0 & 0 & 0 & \frac{e^{ln[H_2RPO_4]}}{ln[H_2RPO_4]} & \frac{e^{ln[HRPO_4^-]}}{ln[HRPO_4^-]} & \frac{e^{ln[RPO_4^{2-}]}}{ln[RPO_4^{2-}]} & \frac{e^{ln[HNaRPO_4]}}{ln[HNaRPO_4]} & \frac{e^{ln[NaRPO_4^-]}}{ln[NaRPO_4^-]} & \frac{e^{ln[Na_2RPO_4]}}{ln[Na_2RPO_4]} & 0 & 0 & 0 & 0 & 0 \\
0 & 0 & 0 & 0 & 0 & 0 & 0 & 0 & 0 & 0 & \frac{e^{ln[CO_{2,aq}]}}{ln[CO_{2,aq}]} & \frac{e^{ln[HCO_3^-]}}{ln[HCO_3^-]} & \frac{e^{ln[CO_3^{2-}]}}{ln[CO_3^{2-}]} & \frac{e^{ln[NaHCO_3]}}{ln[NaHCO_3]} & \frac{e^{ln[NaCO_3^{\square}]}}{ln[NaCO_3^-]} \\
\frac{e^{ln[H^+]}}{ln[H^+]} & \frac{e^{ln[Na^+]}}{ln[Na^+]} & -\frac{e^{ln[Cl^-]}}{ln[Cl^-]} & -\frac{e^{ln[OH^-]}}{ln[OH^-]} & 0 & -\frac{e^{ln[HRPO_4^-]}}{ln[HRPO_4^-]} & -2\frac{e^{ln[RPO_4^{2-}]}}{ln[RPO_4^{2-}]} & 0 & -\frac{e^{ln[NaRPO_4^-]}}{ln[NaRPO_4^-]} & 0 & 0 & -\frac{e^{ln[HCO_3^-]}}{ln[HCO_3^-]} & -2\frac{e^{ln[CO_3^{2-}]}}{ln[CO_3^{2-}]} & 0 & -\frac{e^{ln[NaCO_3^-]}}{ln[NaCO_3^-]}
\end{pmatrix} \qquad \textbf{(B11)}
$$

$$
\boldsymbol{C_{ln}} = \begin{pmatrix}
ln[H^+] \\
ln[Na^+] \\
ln[Cl^-] \\
ln[OH^-] \\
ln[H_2RPO_4] \\
ln[HRPO_4^-] \\
ln[RPO_4^{2-}] \\
ln[HNaRPO_4] \\
ln[NaRPO_4^-] \\
ln[Na_2RPO_4] \\
ln[CO_{2,aq}] \\
ln[HCO_3^-] \\
ln[CO_3^{2-}] \\
ln[NaHCO_3] \\
ln[NaCO_3^-]
\end{pmatrix} \qquad \textbf{(B13)}
$$

$$
\mathbf{K}(\boldsymbol{V_B}) = \begin{pmatrix}
ln\,K_w \\
ln\,K_{a1} + ln\,K_{cc}(V_B) \\
ln\,K_{a2} + ln\,K_{cc}(V_B) \\
ln\,K_{d1} + ln\,K_{cc}(V_B) \\
ln\,K_{d2} + ln\,K_{cc}(V_B) \\
ln\,K_{d3} + ln\,K_{cc}(V_B) \\
ln\,K_{a4} \\
ln\,K_{a5} \\
ln\,K_{d4} \\
ln\,K_{d5} \\
c_{NaCl}\left(\frac{V_{NaCl}}{V_0 + V_B}\right) + \upsilon\varrho_P\left(\frac{m_{CNC}}{V_0 + V_B}\right) + c_B\left(\frac{V_B}{V_0 + V_B}\right) \\
c_{HCl}\left(\frac{V_{HCl}}{V_0 + V_B}\right) + c_{NaCl}\left(\frac{V_{NaCl}}{V_0 + V_B}\right) \\
\varrho_P\left(\frac{m_{CNC}}{V_0 + V_B}\right) \\
\left(c_{CO_3^{2-}}^{air} + c_{CO_3^{2-}}^{base}\right)\left(\frac{V_B}{V_0 + V_B}\right) \\
0
\end{pmatrix} \qquad \textbf{(B12)}
$$

Once obtained, it can be shown that the square matrix **M** has a nonzero determinant, which means that the calculation in equation 20 is possible, because the system we consider contains the necessary information to determine the variables we are interested in, and the matrix **M** is invertible. As mentioned above, analytically, this is not possible, but using MATLAB software, it is possible to numerically obtain solutions.

Applying the same calculations to sodium phosphate salt standards requires three further modifications. Firstly, orthophosphate ions contain a third dissociable proton rather than a chemical bond to the particle surface. Therefore, there is another ionic species that requires consideration, meaning the system of equations needs to be expanded by **equation (B14)**.

$$K_{a_3,eff} = K_{a_3}\frac{[NaPO_4^-][H^+]}{[HPO_4^{2-}][Na^+]} \tag{B14}$$

We are assuming here, as illustrated in **Figure 4**, that free, tribasic orthophosphate ions will immediately associate with a sodium ion in the solution to form monosodium phosphate. Also, we are assuming that the concentration of disodium and trisodium phosphate ions is negligible.[11]

Secondly, counterion condensation plays no role for the dissociation of ions, so the correction is no longer relevant here. And thirdly, given the handling of the chemicals, we found the simplest, most reliable standard to prepare solutions from to be sodium dihydrogen phosphate dihydrate, as it is nonhygroscopic and easier to handle than liquid phosphoric acid. Given that the salt is monobasic, it must be considered according to **equation (B8)**, that the salt contains sodium, and the total amount of phosphate in the system is calculated by an adapted version of **equation (B9)-2**.

$$[\Sigma(Phosphate)] = [Phosphate]_0\left(\frac{V_0}{V_0 + V_B}\right) = c_{NaH_2PO_4}\left(\frac{V_{NaH_2PO_4}}{V_0 + V_B}\right) \qquad \textbf{(B9)-2}$$

In **equation (B9)-2**, $c_{NaH_2PO_4}$ and $V_{NaH_2PO_4}$ are concentration and volume of the phosphate salt standard solution to be analysed as a reference.

These changes are reflected in the matrix $\boldsymbol{M^{salt}}$ according to **equation (B15)** and a volume dependent vector $\boldsymbol{K^{salt}(V_B)}$ according to equation **(B16)**, which enable us to numerically find a solution for the logarithmic concentration vector $\boldsymbol{C^{salt}}_{\boldsymbol{ln}}$ (see, **equation (B17)**) according to **equation (25)**.

$$\boldsymbol{M}^{salt} = \begin{pmatrix}
1 & 0 & 0 & 1 & 0 & 0 & 0 & 0 & 0 & 0 & 0 & 0 & 0 & 0 & 0 & 0 \\
1 & 0 & 0 & 0 & -1 & 1 & 0 & 0 & 0 & 0 & 0 & 0 & 0 & 0 & 0 & 0 \\
1 & 0 & 0 & 0 & 0 & -1 & 1 & 0 & 0 & 0 & 0 & 0 & 0 & 0 & 0 & 0 \\
1 & -1 & 0 & 0 & 0 & 0 & -1 & 1 & 0 & 0 & 0 & 0 & 0 & 0 & 0 & 0 \\
0 & 1 & 0 & 0 & 0 & 1 & 0 & 0 & -1 & 0 & 0 & 0 & 0 & 0 & 0 & 0 \\
0 & 1 & 0 & 0 & 0 & 0 & 1 & 0 & 0 & -1 & 0 & 0 & 0 & 0 & 0 & 0 \\
0 & 1 & 0 & 0 & 0 & 0 & 0 & 0 & 0 & 1 & -1 & 0 & 0 & 0 & 0 & 0 \\
1 & 0 & 0 & 0 & 0 & 0 & 0 & 0 & 0 & 0 & 0 & -1 & 1 & 0 & 0 & 0 \\
1 & 0 & 0 & 0 & 0 & 0 & 0 & 0 & 0 & 0 & 0 & 0 & -1 & 1 & 0 & 0 \\
0 & 1 & 0 & 0 & 0 & 0 & 0 & 0 & 0 & 0 & 0 & 0 & 1 & 0 & -1 & 0 \\
0 & 1 & 0 & 0 & 0 & 0 & 0 & 0 & 0 & 0 & 0 & 0 & 0 & 1 & 0 & -1 \\
0 & \frac{e^{ln[Na^+]}}{ln[Na^+]} & 0 & 0 & 0 & 0 & 0 & \frac{e^{ln[NaPO_4^{2-}]}}{ln[NaPO_4^{2-}]} & \frac{e^{ln[NaH_2PO_4]}}{ln[NaH_2PO_4]} & \frac{e^{ln[NaHPO_4^-]}}{ln[NaHPO_4^-]} & 2\frac{e^{ln[Na_2HPO_4]}}{ln[Na_2HPO_4]} & 0 & 0 & 0 & \frac{e^{ln[NaHCO_3]}}{ln[NaHCO_3]} & \frac{e^{ln[NaCO_3^-]}}{ln[NaCO_3^-]} \\
0 & 0 & \frac{e^{ln[Cl^-]}}{ln[Cl^-]} & 0 & 0 & 0 & 0 & 0 & 0 & 0 & 0 & 0 & 0 & 0 & 0 & 0 \\
0 & 0 & 0 & 0 & \frac{e^{ln[H_3PO_4]}}{ln[H_3PO_4]} & \frac{e^{ln[H_2PO_4^-]}}{ln[H_2PO_4^-]} & \frac{e^{ln[HPO_4^{2-}]}}{ln[HPO_4^{2-}]} & \frac{e^{ln[NaPO_4^{2-}]}}{ln[NaPO_4^{2-}]} & \frac{e^{ln[NaH_2PO_4]}}{ln[NaH_2PO_4]} & \frac{e^{ln[NaHPO_4^-]}}{ln[NaHPO_4^-]} & \frac{e^{ln[Na_2HPO_4]}}{ln[Na_2HPO_4]} & 0 & 0 & 0 & 0 & 0 \\
0 & 0 & 0 & 0 & 0 & 0 & 0 & 0 & 0 & 0 & 0 & \frac{e^{ln[CO_{2,aq}]}}{ln[CO_{2,aq}]} & \frac{e^{ln[HCO_3^-]}}{ln[HCO_3^-]} & \frac{e^{ln[CO_3^{2-}]}}{ln[CO_3^{2-}]} & \frac{e^{ln[NaHCO_3]}}{ln[NaHCO_3]} & \frac{e^{ln[NaCO_3^{\square}]}}{ln[NaCO_3^-]} \\
\frac{e^{ln[H^+]}}{ln[H^+]} & \frac{e^{ln[Na^+]}}{ln[Na^+]} & -\frac{e^{ln[Cl^-]}}{ln[Cl^-]} & -\frac{e^{ln[OH^-]}}{ln[OH^-]} & 0 & -\frac{e^{ln[H_2PO_4^-]}}{ln[H_2PO_4^-]} & -2\frac{e^{ln[HPO_4^{2-}]}}{ln[HPO_4^{2-}]} & -2\frac{e^{ln[NaPO_4^{2-}]}}{ln[NaPO_4^{2-}]} & 0 & -\frac{e^{ln[NaHPO_4^-]}}{ln[NaHPO_4^-]} & 0 & 0 & -\frac{e^{ln[HCO_3^-]}}{ln[HCO_3^-]} & -2\frac{e^{ln[CO_3^{2-}]}}{ln[CO_3^{2-}]} & 0 & -\frac{e^{ln[NaCO_3^-]}}{ln[NaCO_3^-]}
\end{pmatrix} \tag{B15}$$

$$\boldsymbol{C}^{salt}{}_{\boldsymbol{ln}} = \begin{pmatrix}
ln[H^+] \\
ln[Na^+] \\
ln[Cl^-] \\
ln[OH^-] \\
ln[H_3PO_4] \\
ln[H_2PO_4^-] \\
ln[HPO_4^{2-}] \\
ln[NaPO_4^{2-}] \\
ln[NaH_2PO_4] \\
ln[NaHPO_4^-] \\
ln[Na_2HPO_4] \\
ln[CO_{2,aq}] \\
ln[HCO_3^-] \\
ln[CO_3^{2-}] \\
ln[NaHCO_3] \\
ln[NaCO_3^-]
\end{pmatrix} \tag{B17}$$

$$\boldsymbol{K}^{salt}(\boldsymbol{V_B}) = \begin{pmatrix}
ln\ K_w \\
ln\ K_{a1} \\
ln\ K_{a2} \\
ln\ K_{a3} \\
ln\ K_{d1} \\
ln\ K_{d2} \\
ln\ K_{d3} \\
ln\ K_{a4} \\
ln\ K_{a5} \\
ln\ K_{d4} \\
ln\ K_{d5} \\
c_{NaCl}\left(\frac{V_{NaCl}}{V_0 + V_B}\right) + \upsilon \varrho_P \left(\frac{m_{CNC}}{V_0 + V_B}\right) + c_B\left(\frac{V_B}{V_0 + V_B}\right) \\
c_{HCl}\left(\frac{V_{HCl}}{V_0 + V_B}\right) + c_{NaCl}\left(\frac{V_{NaCl}}{V_0 + V_B}\right) \\
\varrho_P\left(\frac{m_{CNC}}{V_0 + V_B}\right) \\
\left(c^{air}_{CO_3^{2-}} + c^{base}_{CO_3^{2-}}\right)\left(\frac{V_B}{V_0 + V_B}\right) \\
0
\end{pmatrix} \tag{B16}$$

Appendix C: Ion densities in the diffuse layer and bulk activities

Even though they are dissociated from the surface groups, significant amounts of hydrated ions associate in a diffuse layer around the particle surface rather than separating from the particles altogether.[12] This reduction in bulk cation activity has a measurable impact on the conductivity. Therefore, it is mandatory to take a closer look at the structure of the electrostatic double layer around the particles, which is shown schematically in **Figure 6** and **Figure 7**.[12] Given the impact on the conductance, Jellium models do not apply here.[10, 13]

Instead, we need to consider a geometric framework around the particles to describe the extent of the diffuse layer. In this study, we interpret the boundary between Stern layer and Guoy-Chapman (diffuse) layer as the closest distance, up to which a hydrated ion can approach the surface of the particle. In keeping with the Debye-Hückel theory[7], where ions are considered as voluminous spheres with point charges in their center, this means that the Guoy-Chapman layer begins at a distance $r_P + r_{ion}$ from the center of the cylindrical particles. This is in reasonable agreement with molecular dynamics simulations.[14]

A boundary between diffuse layer and bulk phase is less easily defined. Phenomenologically, this boundary is identified as the slipping plane, located at the distance from the surface, at which the potential has decreased to the observed zeta potential of the particle.[15] The zeta potential, in turn, is commonly quantified by the mobility of the particles in an external electrical field.[15-17] However, apart from the surface potential and the countercharges, in the presence of an external electric field, the zeta potential is influenced significantly by the dependance of the mobility on the polarization of the double layer in the electric field as well as the surrounding mobile counterions.[16-18] The polarization gives rise to the relaxation effect, an effective decrease in the field strength experienced by the particle, which is represented in **Figure C1**, whereas the electrophoretic effect attributes a further reduction in mobility of the particles to the stream of mobile counterions and associated solvent molecules in the opposite direction.[18]

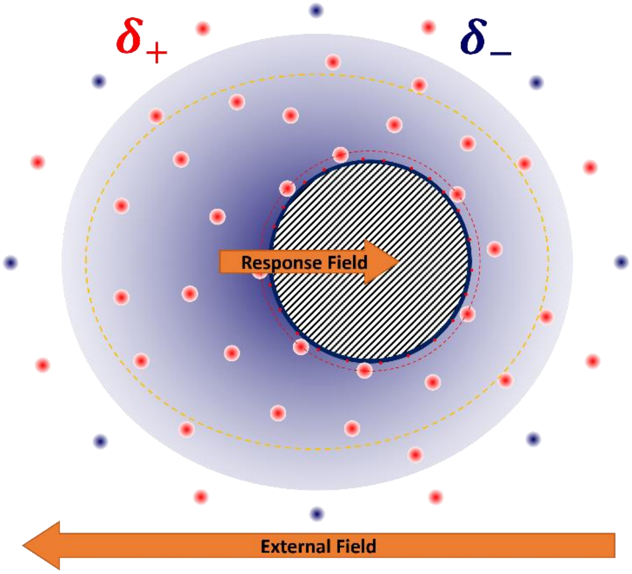

Figure C1. Schematic representation of the relaxation effect. The polarization of the ionic atmosphere generates a response field in opposition to the external field, which in sum reduces the strength of the external field.

As such, the zeta potential is a function of the surface charge, the attracted counterions in the diffuse layer, as well as the ionic strength of the medium and it is generally observed through measurements, rather than predicted. Such measurements are impractical for our purpose, as it would require constant monitoring of the zeta potential throughout the titration. Instead, we will assume that the boundary of the diffuse layer is found at that distance from the particle center, where the surface potential has decreased to the level of the thermal potential ($\psi(r_B) = -\frac{k_b T}{q_e}$). At room temperature, the thermal potential corresponds to roughly -26 mV, which is in the same range as the observed zeta potentials in the presence of background electrolyte.[1] Additionally, we find that recalculating with a boundary potential of $-2\frac{k_b T}{q_e}$, representing the other end of the range of reported zeta potential values[1], has a negligible impact on the calculated bulk ion concentrations. Works on charge normalization consider Wigner-Seitz cells boundaries that follow from the particle density.[9] This methodology is somewhat less helpful here, as we rely on a cutoff distance, at which we can consider the ionic conductivity as unimpeded. Compared to the cited works on charge renormalization, our approach echoes the consideration of smaller Wigner-Seitz cells ending at the boundary layer, which are in contact with a reservoir, that holds the bulk ions.[19, 20] With these boundary conditions, we can apply the Poisson-Boltzmann equation as follows:

According to Debye and Hückel, and based on the Boltzmann principle, for a solution with exclusively monovalent ions, the charge density close to the charged particle, can be described with **equation (C1)**.[7]

$$\begin{aligned}\varrho(r) &= \sum_i \varrho_i(r) \\ &= \sum_m \varrho_{+,m}(r) + \sum_n \varrho_{-,n}(r) \qquad \textbf{(C1)} \\ &= \sum_m \varrho_{+,m}^{bulk}\, e^{-\frac{q_e \Psi(r)}{k_B T}} - \sum_n \varrho_{-,n}^{bulk}\, e^{\frac{q_e \Psi(r)}{k_B T}}\end{aligned}$$

$$= I^{bulk}\left(e^{-\frac{q_e\Psi(r)}{k_BT}} - e^{\frac{q_e\Psi(r)}{k_BT}}\right)$$

Here, $\varrho(r)$ is the charge density at a radial distance r from the central axis of the cylindrical particle, $\varrho_{+,m}(r)$ is the charge density caused by cation m, $\varrho_{-,n}(r)$ is the (negative) charge density caused by anion n and I^{bulk} is the bulk ionic strength.

Our system contains divalent carbonate ions at elevated pH, which are not accurately reflected in **equation (C1)**. Instead, the correct term to calculate the ion density of carbonate ions is presented in **equation (C2)**.[7]

$$\varrho_{CO_3^{2-}}(r) = z^2\varrho_{CO_3^{2-}}^{bulk}e^{\frac{zq_e\Psi(r)}{k_BT}} = 4\varrho_{CO_3^{2-}}^{bulk}e^{\frac{2q_e\Psi(r)}{k_BT}} = 4\cdot\varrho_{CO_3^{2-}}^{bulk}\left(e^{\frac{q_e\Psi(r)}{k_BT}}\right)^2 \qquad \textbf{(C2)}$$

Given the low concentration of carbonate ions in the solution and the fact that the ions are repelled from the surface, the error in treating carbonate ions as four separate, singly charged moieties described by **equation (C1)** is negligible, but significantly simplifies solving this new system of equations.

The charge density in the Guoy-Chapman layer is given by the Poisson-Boltzmann equation, expressed in equation **(C3)** in cylindrical coordinates[21]:

$$\frac{d^2\Psi}{dr^2} + \frac{1}{r}\frac{d\Psi}{dr} = -\frac{\varrho(r)}{\varepsilon_0\varepsilon_r} \qquad \textbf{(C3)}$$

Here, Ψ is the surface potential.

The is a significant distinction between these two equations is that the ion density in **equation (C1)** is based on the ionic strength. Therefore, it differs from the charge density in **equation (C3)** if multivalent ions are present. The charge density is the difference between anion and cation density. This separation of charges is evidence of an electric field and is therefore considered in the potential decrease described by **equation (C3)**.

The first-order term in **equation (C3)** relates to the curvature of the particle surface. Given the curvature, comparatively simple, linear solutions for the potential based on exponential functions do not apply here. Instead, the system can be described using Bessel functions.

Oshima, Healy and White[16] integrated **equation (C3)** after normalizing the potential and the particle radius by thermal units and the Debye length, respectively. Their expression for the potential as a function of radial distance from the particle axis is given in **equation (C4)**.

$$y(r) = 2\ln\left(\frac{\big(1 + Dc(r)\big)\left(1 + \left(\frac{1-\beta}{1+\beta}\right)Dc(r)\right)}{\big(1 - Dc(r)\big)\left(1 - \left(\frac{1-\beta}{1+\beta}\right)Dc(r)\right)}\right) \qquad \textbf{(C4)}$$

with

$$\beta = \frac{K_0(\kappa r_p)}{K_1(\kappa r_p)} \qquad \textbf{(C4)-a}$$

$$c(r) = \frac{K_0(\kappa r)}{K_0(\kappa r_p)} \qquad \textbf{(C4)-b}$$

$$D = \frac{(1+\beta)\tanh\left(\frac{y_0}{4}\right)}{1 + \sqrt{1 - (1-\beta^2)\left(\tanh\left(\frac{y_0}{4}\right)\right)^2}} \qquad \textbf{(C4)-c}$$

$$y_0 = \frac{q_e \Psi_0}{k_B T} = \pm 2\ \cosh^{-1}\left(-\frac{1}{\kappa r_p} + \sqrt{\left(\frac{1}{\kappa r_p}\right)^2 + \left(\frac{\sigma}{\sqrt{8 I^{bulk} \varepsilon_0 \varepsilon_r k_B T}}\right)^2 + \frac{1}{2}}\right) \qquad \textbf{(C4)-d}$$

In these equations, $y(r)$ is the normalized surface potential, obtained from the real surface potential by comparison with the thermal potential, y_0 is the normalized surface potential, which, in our case has a negative sign, and $K_0(x)$ and $K_1(x)$ refer to the modified Bessel functions of the second kind of order 0 and 1.

This potential expression gives access to the ion densities in the immediate vicinity of the particle, which in turn enables balancing the distribution of dissociated ions in the system by distinguishing quantitatively between bulk ions and those kinetically tied to the particle.[22]

With the knowledge of the exact surface charge at any given point on the titration curve according to **equation (14)**, the potential around the particles can be calculated with **equation (C4).**

$$\begin{aligned} n_i^{edl} &= \int_{r_p+r_{ion,i}}^{r_B} \left(\varrho_i^{bulk} e^{-z_i y(r)}\right) dV = \int_{r_p+r_{ion,i}}^{r_B} \left(\varrho_i^{bulk} e^{-z_i y(r)}\right) 2\pi l_{total} r dr \\ &= 2\pi l_{total} \varrho_i^{bulk} \cdot \int_{r_p+r_{ion,i}}^{r_B} r e^{-z_i y(r)} dr \end{aligned} \quad \textbf{(C5)}$$

Here, n_i^{edl} is the amount of ion i in the diffuse layer, ϱ_i^{bulk} and z_i are the bulk ion densities and charge valencies of ion i, which in this study, specifically, are +1 for cations and -1 for anions and l_{total} is the combined length of all CNC in the system placed end-to-end.

Equation (C5) yields total numbers of ions that are found in the volume around the nanocellulose particles at distances $r_{ion} < r < r_B$ from the particle surface at r_p from the particle axis. By balancing with the total number of dissociated ions in the system, n_i^{total}, it becomes possible to determine the ionic strength, as well as the amounts of the separate ionic species in the bulk phase , n_i^{bulk}, with the bulk phase being located at distances $r > r_B$from any particle surface. This is described by **equation (C6)**.

$$\begin{aligned} n_i^{bulk} &= n_i^{total} - n_i^{edl} \\ &= (V_0 + V_B)\varrho_i^{total} - n_i^{edl} \end{aligned} \tag{C6}$$

Equations (C5) to **(C6)** refer to every individual ionic species in the solution, given that the lower integration limit contains the individual ion radii $r_{ion,i}$. Given this challenge, and accepting that it may misrepresent the system slightly, we will assume that the closest distance, to which any ion can approach the particle surface, is the radius of a hydrated sodium ion, r_{Na^+}, which has been determined as 250 pm. Chloride, hydroxide and carbonate ions are repelled from the surface, so either ions concentrations will be negligible at the boundary between the Stern and Gouy-Chapman layers, rendering this approximation viable, and given the diffusion by proton hopping, defining a set radius for protons is difficult. Therefore, the simplest solution is to assume a similar radius to that of sodium ions, which is similar to that of an expected oxonium ion.

With these assumptions and with the knowledge of the total amount of ions in double layer and bulk phase of the analyte based on the solution to **equation (25)**, it becomes possible to calculate the number of cations and anions in the double layer by solving **equation (C7)** for the individual cationic and anionic species. These numbers of ions can then be converted into activity coefficients and concentrations according to **equation (C8)**.

$$n_i^{edl} = 2\pi l_{total}\varrho_i^{bulk} \cdot \int_{r_p + r_{Na^+}}^{r_B} r e^{-z_i y(r)} dr \tag{C7}$$

$$\gamma_i = \frac{n_i^{bulk}}{n_i^{total}} = \frac{\varrho_i^{bulk}}{\varrho_i^{total}} = \frac{c_i^{bulk}}{c_i^{total}} \tag{C8}$$

It is worth noting that in **equation (C8)**, the (relative) bulk activities for ions with equal charge should be identical, as the attraction of ions into the double layer depends solely on charge. This is evident when **equations (C8)** and **(C7)** are combined to yield the number balances of cations and anions (**equation (C9)**) and a direct expression for the bulk activity of cations and anions (**equation (C10)**).

$$n_i^{total} = n_i^{bulk} + n_i^{edl} = n_i^{bulk} + \frac{n_i^{bulk}}{(V_x + V_b)} 2\pi l_{total} \cdot \int_{r_p + r_{Na^+}}^{r_B} r e^{-z_i y(r)} dr \tag{C9}$$

$$\begin{aligned} \gamma_i = \frac{n_i^{bulk}}{n_i^{total}} &= \frac{1}{1 + \frac{2\pi l}{(V_x + V_b)} \cdot \int_{r_p + r_{Na^+}}^{r_B} r e^{-z_i y(r)} dr} \\ &= \frac{(V_x + V_b)}{(V_x + V_b) + 2\pi l_{total} \cdot \int_{r_p + r_{Na^+}}^{r_B} r e^{-z_i y(r)} dr} \end{aligned} \tag{C10}$$

The only dependence of the bulk activities for cations and anions, according to **equation (C10)**, is on the decreasing surface potential throughout the diffuse layer, which in turn is a function of the surface charge and the bulk ionic strength (see, **equation (C4)**). Given this dependance of the individual ionic activities on the sum of all bulk ion concentrations, again, the equations cannot be solved individually or analytically. Instead, we consider the following system of equations derived from **(A3)**, **(C4)** and **(C9)**, which can be solved numerically.

$$\kappa = \sqrt{\frac{2{q_e}^2 N_A I}{\varepsilon_0 \varepsilon_r k_B T}} = \sqrt{\frac{2{q_e}^2 N_A}{\varepsilon_0 \varepsilon_r k_B T} \sum_i \frac{z_i^2 n_i^{bulk}}{(V_0 + V_B)}} \tag{C11)-(1}$$

$$n_i^{bulk} = n_i^{total} - \frac{n_i^{bulk}}{(V_0 + V_B)} 2\pi l_{total} \cdot \int_{r_p + r_{Na^+}}^{r_B} r e^{-z_i y(r)} dr \tag{C11)-(12}$$

$$n_i^{total} = (V_0 + V_B) \varrho_i^{total} \tag{C11)-(13}$$

$$\varrho_i^{bulk} = \frac{n_i^{bulk}}{(V_0 + V_B)} \tag{C11)-(14}$$

Here, **equation (C11)-1** describes the Debye length as a function of the bulk ionic strength, which is applied in the calculation of the surface potential according to **equation (C4)**. Integrating **equation (C4)** in the range of the diffuse layer then allows for the determination of the number density of ions in the bulk phase, which can be converted to bulk ion densities using the overall volume of the bulk solution (**equation(C11)-14**). The input required to solve this equation is the total number of ions distributed between bulk phase and diffuse layer, which is obtained in **equation (C11)-1-3** using the ion total densities calculated in **equation (25)**. The unit of the ion densities is mol/m^3, which is equivalent to mmol/L.

Appendix D: Conductivity of the colloidal particles

The conductivity of dissolved polyelectrolytes has previously been calculated for polymer chains.[23] This model is derived from an idealized view of the polymers as infinitely long cylinders with a homogenous line charge. Previously published by Manning[24], van Leeuwen et al.[23] adapted the same deliberations in SI-units rather than the cgs system and applied Manning's theorem to experimental values. The starting point for calculating the polyelectrolyte mobility is the Henry equation for the mobility of randomly oriented, infinitely long cylinders (**equation (D1)**).

$$u'_p \approx u_{p,eff} = \frac{2}{3}\frac{\varepsilon_0 \varepsilon_r}{\eta}\zeta \qquad \textbf{(D1)}$$

Here, u'_p is the idealized particle mobility observed if no polarization would occur, $u_{p,eff}$ is the effective particle mobility, η is the viscosity of water at room temperature and ζ is the observed zeta potential.

Henry's equation relates the zeta potential to the electrophoretic particle mobility.[23-25] Inconveniently, the zeta potential is not equal to the surface potential of the considered particles and as mentioned above, there is no direct theoretical access to Zeta potential values.[23] Henry's equation considers the friction between particle and solvent, but neglects relaxation effects caused by the external electric field. The external field causes a polarization in the counterion distribution around the particles which generates an opposing electrical field as shown in **Figure C1**. As a result, the particle is partially shielded from the external potential.[25]

Therefore, as a correction to Henry's equation, Manning considers the diminished, effective potential based on the flux of the free counterions compared to that of the counterions in the double layer, which are diffusing with the particle. According to van Leeuwen et al., these considerations can be expressed as **equations (D2)** and **(D3)**.

$$\frac{E_{eff}}{E} = \gamma_p - (1 - \gamma_p)\frac{u_{p,eff}}{\mu_+} \tag{D2}$$

$$\frac{u'_p}{E} = \frac{u_{p,eff}}{E_{eff}} \tag{D3}$$

Here, E is the strenght of the external field, E_{eff} is the effective external electrical field taking into account the polarization of the diffuse layer, γ_p is the degree of dissociation of the surface groups of the particles and μ_+ is the average mobility of the counterions.

In these considerations, γ is an activity coefficient that describes the fraction of freely dissociated ions as opposed to $(1 - y)$, which describes the fraction of counterions trapped in the double layer around the particle. Citing the result of a series development of an expression describing the field around a real polyion and experiments that confirmed the value, Manning and van Leeuwen et al. assume a value of $\gamma = 0.866$.[23, 24]

Combining **equations (D1)-(D3)** yields **equation (D4)**.

$$u_{p,eff} = \frac{\gamma_p \frac{2}{3}\frac{\varepsilon_0 \varepsilon_r}{\eta}|\zeta|}{1 + \frac{(1-\gamma_p)}{\mu_+}\frac{2}{3}\frac{\varepsilon_0 \varepsilon_r}{\eta}|\zeta|} \tag{D4}$$

This expression still depends on the zeta potential ζ, which Manning, considering polyelectrolytes in otherwise ion-free environment, estimates as the limiting potential according to the Debye-Hückel theory. For monovalent counterions, this estimation can be expressed in the form of **equation (D5)**.[24]

$$\zeta = 2\frac{k_B T}{\epsilon}\ln\left(k'_D r_{particle}\right) \tag{D5}$$

with

$$k'_D = \sqrt{\frac{{q_e}^2 c_p}{\varepsilon_0 \varepsilon_r k_B T}} \tag{D5)a}$$

The inverse Debye length k'_D in this case only depends on the concentration of charged groups on the particle c_p, because it is assumed that apart from the dissociated polyelectrolyte, the solution is otherwise ion-free.

Combining **equations (D4)** and **(D5)** and multiplying with the Faraday constant, an expression can be derived for the molar electrolytic conductivity of the particle's surface groups (**equation (D6)**):

$$\Lambda_P = \frac{\gamma_p \Lambda_+ H \ln\left(k'_D r_{particle}\right)}{\Lambda_+ + (1-\gamma_p) H \ln\left(k'_D r_{particle}\right)} \tag{D6}$$

with

$$H = \frac{4}{3}\frac{\varepsilon_0 \varepsilon_r}{\eta} RT \tag{D6)a}$$

These equations are not directly applicable to our model given that, as mentioned in Appendix C, it is impractical to determine zeta potentials along the titration process and we therefore considered a boundary potential of -26 mV instead. Additionally, the estimate for the zeta potential does not apply to our particles, as the Debye length in our system is neither significantly bigger nor smaller than the particle radius. Instead, both values are very similar throughout the titration, and the fact that the Debye length decreases to the exact value of the particle radius and below during the addition of excess sodium hydroxide in the end of the titration makes the estimate mathematically impractical. When Debye length and particle radius coincide, the logarithmic term takes the value 0, rendering the estimated particle mobility value 0 as well.

Therefore, we choose to adapt **equation (D4)** by replacing the zeta potential with our boundary potential (see, **Appendix C**) and by applying the activity values that follow from the bulk concentrations calculated in Appendix C. In so doing, we obtain **equations (D7)** and **(D8)**.

$$u_{p,eff} = \frac{\gamma_p \frac{2}{3}\frac{\varepsilon_0 \varepsilon_r}{\eta}\left|-\frac{k_B T}{q_e}\right|}{1 + \frac{\left(1-\gamma_p\right)}{\mu_+}\frac{2}{3}\frac{\varepsilon_0 \varepsilon_r}{\eta}\left|-\frac{k_B T}{q_e}\right|} \tag{D7}$$

$$\Lambda_{p,eff} = F u_{p,eff} = \frac{\gamma_p \lambda_+ H}{\lambda_+ + \left(1-\gamma_p\right) H} \tag{D8}$$

with

$$H = \frac{4}{3}\frac{\varepsilon_0 \varepsilon_r R T}{\eta} \tag{D8)a}$$

and

$$\Lambda_+ = \frac{c_{H^+}\Lambda^0_{H^+} + c_{Na^+}\Lambda^0_{Na^+}}{c_{H^+} + c_{Na^+}} \tag{D8)b}$$

The molar equivalent conductivities $\Lambda_{p,eff}$ of the particles is obtained by multiplying the particle mobility $u_{p,eff}$ with the Faraday constant F.

Finally, in addition to the particles moving through the solution and adding to its conductivity, the ions in the double layer are not stagnant.[26] Instead, there is a fluid exchange between ions in the diffuse layer and those in bulk that amounts to a net zero change in ionic distribution, but as ions enter and leave the diffuse layer, a net charge transport is possible. In literature, theses phenomena have been summarized as surface conductivity.[27] Given the dominant influence of the charged particle surface, however, this charge transport due to the diffuse layer is lower than that through the bulk phase. Rather than following the direction of the external field applied to measure conductivity, the primary movement of the ions in the diffuse layer is radial with regard to the cylindrical charged particle. Following the deliberations outlined by Dhukin, Zimmermann and Werner[27], the surface conductivity of the ions can be scaled by comparing the electrostatic energy in bulk and that in the double layer according to **equation (D9)**.

$$\begin{aligned}\Lambda_{+,s} &= \Lambda_+ \frac{2\pi l_{particle}\varrho_i^{bulk}\cdot\int_{r_{particle}+r_{Na^+}}^{r_B} re^{0}dr}{2\pi l_{particle}\varrho_i^{bulk}\cdot\int_{r_{particle}+r_{Na^+}}^{r_B} re^{-z_i y(r)}dr} \\ &= \lambda_+ \frac{\pi l_{particle}\left({r_B}^2-{r_{particle}}^2\right)}{2\pi l_{particle}\int_{r_{particle}+r_{Na^+}}^{r_B} re^{-y(r)}dr}\end{aligned} \qquad \textbf{(D9)}$$

Alphabetical list of symbols

Constants

F	Faraday constant $F = q_e N_A = 96485\ \frac{C}{mol}$
k_B	Boltzmann constant $1.38\cdot 10^{-23}\ \frac{J}{K}$
N_A	Avogardro’s number: $6.023\cdot 10^{23}\ \frac{1}{mol}$

q_e	Elementary charge $-1.602 \cdot 10^{-19}\ C$
ε_0	Vacuum permittivity $8.85 \cdot 10^{-12}\ \frac{C^2}{Jm}$
ε_r	Relative permittivity; water at room temperature: 78
λ_B	Bjerrum length; in water at room temperature: $7.15 \cdot 10^{-10}\ m$
η	Viscosity of water, at 20°C: 1.002 mPas

Latin alphabet symbols

A1	Acid dissociation reaction of orthophosphoric acid
A2	Acid dissociation reaction of dihydrogen phosphate
A3	Acid dissociation reaction of hydrogen phopshate
A4	Acid dissociation reaction of Carbonic acid
A5	Acid dissociation reaction of bicarbonate
A6	Acid dissociation reaction of sodium dihydrogen phosphate
A_P	Total surface area
A_{ch}	Area of a single charge on the surface
A_{el}	Electrode area
c_B	Concentration of the titrant (NaOH, 0.1 mM)
$\boldsymbol{c}(\boldsymbol{V_B})$	Vector containing the real overall concentrations of dissociated ions at titrant volume $\boldsymbol{V_B}$
$\boldsymbol{c^{bulk}}(\boldsymbol{V_B})$	Vector containing the real bulk concentrations of dissociated ions at titrant volume $\boldsymbol{V_B}$
$\boldsymbol{C_{ln}^{bulk}}(\boldsymbol{V_B})$	Vector of logarithmic bulk concentrations at titrant volume $\boldsymbol{V_B}$ (see, equations (B13) and (B17))
$\boldsymbol{C_{ln}}(\boldsymbol{V_B})$	Vector of logarithmic overall concentrations at titrant volume $\boldsymbol{V_B}$ (see, equations (B13) and (B17))
Δc_B	Titrant concentration change in the analyte
$c_{CO_3}^{NaOH}$	Concentration of carbonate in the titrant
$c_{CO_3}^{air}$	Virtual concentration of carbonate entering the analyte from the

	air
c_{HCl}	Concentration of HCl solution (0.1 mM)
$c_{NaH_2PO_4}$	Concentration of sodium dihydrogen phosphate in the standard solution
$c_{P,analyte}$	Mass concentration of phosphate in the substituted cellulose
$[Carbonate]_{NaOH}$	Concentration of carbonate in the titrant
$[Carbonate]_{air}$	Perceived concentration of carbonate in the titrant, i.e. amount of carbonate entering the analyte per titrant Volume increment
D1	Sodium dissociation reaction of sodium dihydrogen phosphate
D2	Sodium dissociation reaction of sodium hydrogen phosphate
D3	Sodium dissociation reaction of disodium hydrogen phosphate
D4	Sodium dissociation reaction of sodium bicarbonate
D5	Sodium dissociation reaction of sodium carbonate
$d_{arc_{\perp}}$	Rectangular component of an arc length spanning an area increment
d_{3D}	3-dimensional Euclidian distance of any surface point from the origin
dA_i	Area increment i
d_{arc}	Arc length increment
d_{charge}	Radius of the considered charged moiety
d_{el}	Electrode distance
d_{xy}	Two-dimensional Euclidian distance of any surface point from the z-axis
E	Externally applied electrostatic potential for mobility measurements
E_{eff}	Effective external potential at the particle boundary plane
eq	Equivalents of base added to the analyte (NaOH)
G	Conductance $[S]$

G_{norm}	Normalized conductance $[Sm^2]$
$\Delta G^0_{dissociation}$	Ion pair dissociation reaction free energy
ΔG^0_{total}	Total Gibbs free energy
I	Bulk ion density $\left[\frac{1}{m^3}\right]$
I^{bulk}	Bulk ionic strenght
$K_0(x)$, $K_1(x)$	Modified Bessel functions of the second kind of order 0 and 1
$K_{condensation}$	Counterion condensation contribution to dissociation equilibrium
$K_{condensation}$	Constant expressing the influence of counterion condensation
$K_{dissociation}$	Ion pair dissociation equilibrium constant
K_j	Equilibrium constant of reaction j (see, Table 1)
K_{new}	Corrected overall equilibrium constant
$\boldsymbol{K(V_B)}$	Vector containing the system information at titrant volume $\boldsymbol{V_B}$ as defined in equations (B12) and (B16)
l	Particle length
$\boldsymbol{M}$	Matrix $\boldsymbol{M}$ as defined in equations (B11) and (B15)
$\boldsymbol{M^{-1}}$	inverse of the Matrix $\boldsymbol{M}$
$m_{analyte}$	Mass of cellulose in the analyte
m_p	Total mass of cellulose in the analyte
$N_{q,i}$	Number of elementary charges in area increment i
N_q	Number of elemental charges generating the electrostatic potential
N_q	Total number of charge equivalents
n_{HCl}	Amount of HCl used to acidify the analyte
$n_{Phosphate}$	Amount of phosphate in the analyte
n_{base}	Amount of added base (NaOH)

Δn_B	Change in titrant amountin the analyte
$n_{carbonate}$	Amount of carbonate in the analyte
n_i^{bulk}	Amount of ion i in the bulk phase
n_i^{edl}	Amount of ion i in the diffuse layer
n_i^{total}	Total amount of ion i in the analyte
q_i	Charge i $[C]$
q_{probe}	Probing charge experiencing
$\overset{\rightarrow}{r_i}$	Location vector of a specific charge i
$r_{Carbonation}$	Reaction rate of the carbonation reaction
r_{ion}	Ion radius
r_p	Particle radius
T	Temperature $[K]$
U	Electrostatic potential energy $[J]$
U_{site}	Electrostatic potential energy of the environment at the considered site
u'_p	Average mobility of the cellulose particles in standard conditions
$u_{p,eff}$	Observed mobility of the cellulose particles affected by relaxation
V_B	Volume of added titrant (NaOH)
$V_{NaH_2PO_4}$	Volume of sodium dihydrogen phosphate added to the analyte
V_{el}	Electrode measuring geometry volume
V_o	Initial volume of the analyte
V_p	Particle volume
X,y,z	Cartesian coordinates to describe the extent of the particles (see, A1)
x_{ch}, y_{ch}, z_{ch}	Extent of the probing charge in the origin of the coordinate

	system in x-, y- and z-direction
y_0	Normalized surface potential
$y(r)$	Normalized potential as a function of radial distance from the particle axis
z_i	Charge valencies of ion i
z_{min}, $z_{max,1}$, $z_{max,2}$	Extent of the particle along the z-axis

Greek alphabet symbols

α	Titer of carbonate in the titrant
γ_i	Bulk activity of ion i
γ_p	Degree of dissociation of the particle surface groups (mol dissociated per mol surface groups)
$\boldsymbol{\gamma}(\boldsymbol{V_B})$	Bulk activity vector at titrant volume $\boldsymbol{V_B}$
$\boldsymbol{\gamma_{ln}}(\boldsymbol{V_B})$	Logarithmic bulk activity vector at titrant volume $\boldsymbol{V_B}$
λ_D	Debye lenght
ζ	Zeta potential
κ	Debye parameter
$\Lambda_{+,s}$	Estimated average molar electrolytic equivalent conductivity of cations in the diffuse layer
Λ_+	Average molar electrolytic equivalent conductivity of the counterions of the particles (here: sodium and protons)
Λ_P	Estimated average molar electrolytic equivalent conductivity of the particles
μ_+	Average mobility of the dissociated counterions
ρ	Density of cellulose
$\varrho(r)$	Overall charge density as a function of radial distance from the particle axis
$\varrho_{CO_3^{2-}}(r)$	Charge density due to carbonate ions

$\varrho_{CO_3^{2-}}^{bulk}$	Bulk charge density due to carbonate
$\varrho_{-,n}(r)$	Charge density due to anion species n
$\varrho_{+,m}(r)$	Charge density due to cation species m
$\varrho_i(r)$	Charge density due to ionic species i as a function of radial distance from the particle axis
ϱ_i^{bulk}	Bulk ion densities of ion i $\left[\frac{mol}{m^3}\right]$
ϱ_i^{total}	Total ion density of ion i in the system $\left[\frac{mol}{m^3}\right]$
σ	Conductivity $\left[\frac{mS}{cm}\right]$
σ_S	Surface charge expressed as number of unit charges per surface area
σ_m	Specific charge density in mol/kg$\left[\frac{mol}{kg}\right]$
$\Delta\sigma_{norm}$	Conductance change
$\Delta\sigma$	Conductivity change
φ	Electrostatic potential of a point charge
Ψ_0	Electrostatic surface potential
$\Psi(z')$	Integral term describing the normalization of the surface charge interactions

References

1. M. Kröger, O. Badara, T. Pääkkönen, I. Schlapp-Hackl, S. Hietala and E. Kontturi, *Biomacromolecules*, 2023, **24**, 1318-1328.
2. R. M. Smith and R. A. Alberty, *The Journal of Physical Chemistry*, 1956, **60**, 180-184.
3. P. G. Daniele, A. De Robertis, C. De Stefano, A. Gianguzza and S. Sammartano, *Journal of Solution Chemistry*, 1991, **20**, 495-515.
4. R. O. James, J. A. Davis and J. O. Leckie, *Journal of Colloid and Interface Science*, 1978, **65**, 331-344.
5. Y. Noguchi, I. Homma and Y. Matsubara, *Cellulose*, 2017, **24**, 1295-1305.
6. O. Ciftja, A. Babineaux and N. Hafeez, *European Journal of Physics*, 2009, **30**, 623.
7. P. H. Debye, Ernst, *Physikalische Zeitschrift*, 1923, **24**, 185-206.
8. G. S. Manning, *The Journal of Physical Chemistry B*, 2007, **111**, 8554-8559.
9. E. Trizac, L. Bocquet, M. Aubouy and H. H. von Grünberg, *Langmuir*, 2003, **19**, 4027-4033.
10. S. Pianegonda, E. Trizac and Y. Levin, *The Journal of Chemical Physics*, 2007, **126**.
11. A. D. Pethybridge, J. D. R. Talbot and W. A. House, *Journal of Solution Chemistry*, 2006, **35**, 381-393.
12. O. Stern, *Zeitschrift für Elektrochemie und angewandte physikalische Chemie*, 1924, **30**, 508-516.
13. E. Trizac and Y. Levin, *Physical Review E*, 2004, **69**, 031403.
14. P. Batys, S. Luukkonen and M. Sammalkorpi, *Physical Chemistry Chemical Physics*, 2017, **19**, 24583-24593.
15. H. Saboorian-Jooybari and Z. Chen, *Results in Physics*, 2019, **15**, 102501.
16. H. Ohshima, T. W. Healy and L. R. White, *Journal of the Chemical Society, Faraday Transactions 2: Molecular and Chemical Physics*, 1983, **79**, 1613-1628.
17. A. V. Delgado, F. González-Caballero, R. J. Hunter, L. K. Koopal and J. Lyklema, *Pure and Applied Chemistry*, 2005, **77**, 1753-1805.
18. H. Cottet, H. Wu and S. A. Allison, *Electrophoresis*, 2017, **38**, 624-632.
19. A. Bakhshandeh, D. Frydel and Y. Levin, *Langmuir*, 2022, **38**, 13963-13971.
20. M. N. Tamashiro, Y. Levin and M. C. Barbosa, *The European Physical Journal B - Condensed Matter and Complex Systems*, 1998, **1**, 337-343.
21. L. G. D'yachkov, *Technical Physics Letters*, 2005, **31**, 204-207.
22. D. Stigter, *Journal of Colloid and Interface Science*, 1975, **53**, 296-306.
23. H. P. v. Leeuwen, R. F. M. J. Cleven and P. Valenta, *Pure and Applied Chemistry*, 1991, **63**, 1251-1268.
24. G. S. Manning, *The Journal of Physical Chemistry*, 1975, **79**, 262-265.
25. A. S. Jayaraman, E. Klaseboer and D. Y. C. Chan, *Journal of Colloid and Interface Science*, 2019, **553**, 845-863.
26. J. Lyklema, H. P. van Leeuwen and M. Minor, *Advances in Colloid and Interface Science*, 1999, **83**, 33-69.
27. S. S. Dukhin, R. Zimmermann and C. Werner, in *Electrical Phenomena at Interfaces and Biointerfaces*2012, pp. 95-126.